Chemical routes to materials

Giant barocaloric effects in natural graphite/polydimethylsiloxane rubber composites

William Imamura[1,2,*] ![ORCID], Erik Oda Usuda[3], Éder Sócrates Najar Lopes[2], and Alexandre Magnus Gomes Carvalho[1,3,4]

[1] Departamento de Engenharia Mecânica, Universidade Estadual de Maringá, Maringá, PR 87020-900, Brazil

[2] Faculdade de Engenharia Mecânica, Universidade Estadual de Campinas, Campinas, SP 13083-860, Brazil

[3] Departamento de Engenharia Química, Universidade Federal de São Paulo, Diadema, SP 09913-030, Brazil

[4] Instituto de Física Armando Dias Tavares, Universidade Do Estado Do Rio de Janeiro, UERJ, Rua São Francisco Xavier, 524, Rio de Janeiro, RJ 20550-013, Brazil

ABSTRACT

Solid-state cooling based on caloric effects is considered a viable alternative to replace the conventional vapor-compression refrigeration systems. Regarding barocaloric materials, recent results show that elastomers are promising candidates for cooling applications around room temperature. However, elastomers are insulating materials, which is a disadvantage that may compromise practical applications, since high heat transfer properties are typically desirable for more efficiency. Herein, barocaloric effects are investigated in natural graphite/polydimethylsiloxane rubber composites (NG/PDMS), in different concentrations of natural graphite. Adding natural graphite to PDMS, the adiabatic temperature change and the isothermal entropy change of the NG/PDMS composites reduce when compared to PDMS, but the composites still remain in giant barocaloric class and achieve an increase up to $\sim$ 500% in thermal diffusivity and thermal conductivity. The results are promising for solid-state cooling based on barocaloric effect because the NG/PDMS composites combine different desired properties and are identified as better or similar among different barocaloric materials reported in the literature.

🖄 Springer

GRAPHICAL ABSTRACT
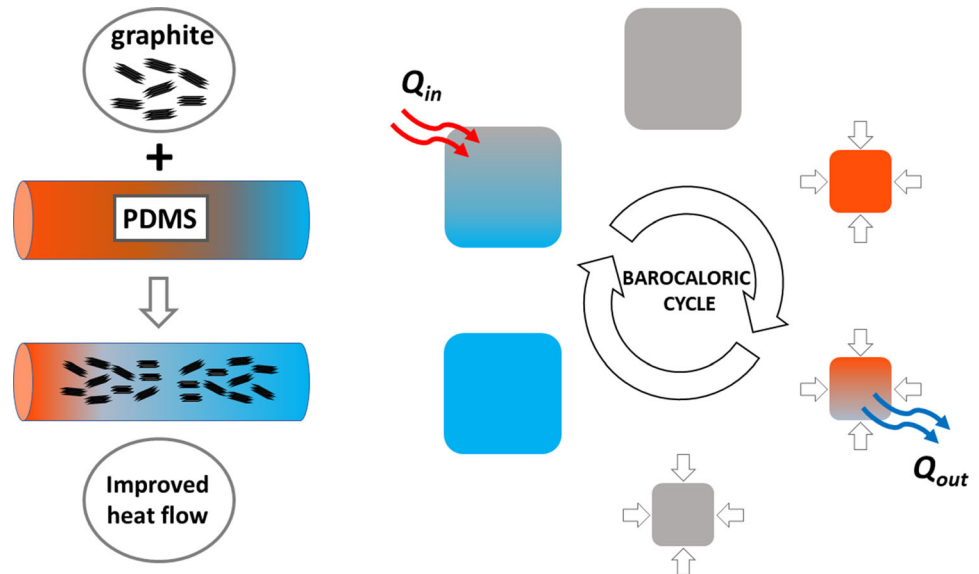
Introduction

The vast majority of artificial cooling technologies are based on vapor-compression cycles of refrigerant fluids, which are environmentally threatening and contribute to 7.8% of the total global greenhouse gas emission [1]. In addition, current cooling technologies present low energy efficiency (< 60% of the Carnot cycle), and their scalability to small dimensions is very limited [1, 2]. Due to these concerns, solid-state cooling appears to be the most promising alternative for next-generation refrigeration technologies.

Solid-state cooling is based on solid materials that present caloric effects and, since the refrigerant is solid, there is a considerable reduction in gas emissions and favors its recyclability. Caloric effect can be described as an adiabatic temperature change (ΔT_S) and an isothermal entropy change (ΔS_T) that a material undergoes when it is subjected to an external field excitation, such as magnetic, electric or mechanic, which giving rise to magnetocaloric, electrocaloric or mechanocaloric effects, respectively. Mechanocaloric effect also includes special cases, and

barocaloric effect (driven by hydrostatic pressure change) is one of them.

Giant barocaloric effects have been reported in a very extensive and diverse range of materials, such as ferroelastic fluorides and oxyfluorides [3–5], intermetallic compounds with magnetostructural transitions [6–11], ferri- and ferroelectrics [12–15], superionic conductors [16, 17], organic–inorganic hybrid perovskites [18–20], spin crossovers materials [21], polymers [22–27], and plastic crystals [28–31]. An ideal barocaloric material must present large $|\Delta S|$ and large $|\Delta T|$ in a wide range of temperature and low-pressure changes, good reversibility, high thermal diffusivity, large density, nontoxicity, and economic and geopolitical availability of the raw materials [32]. However, an ideal barocaloric material does not exist because one or more aspects of interest are negatively affected. Among reported barocaloric materials, elastomer and plastic crystals appear best positioned for a real implementation in cooling devices. The limitations for the applicability of these materials are their low density and low thermal diffusivities [32]. Moreover, plastic crystals still exhibit

large hysteresis and irreversible barocaloric effects for low and moderate pressures [31].

In the present study, we systematically investigated the barocaloric effects in polydimethylsiloxane (PDMS) rubber filled with natural graphite (NG). PDMS rubber[23] was reported with impressive barocaloric properties in a wide range of temperature around room temperature (223–333 K) and low and moderate pressure change (26–390 MPa), but it is affected by low thermal conductivity (~ 0.16 W m^{-1} K^{-1}). It is well-known that several allotropes of carbon (natural graphite, expanded graphite, exfoliated graphite, carbon fibers, carbon nanotubes, graphene, etc.) are extensively used as filler dispersed in a continuous polymer matrix to enhance thermal conductivity [33]. Natural graphite is interesting for the development of barocaloric composites because it has high values of thermal conductivity (70–220 W m^{-1} K^{-1}) [34], it is inert, nontoxic, and also it is a very low price raw material (500–800 US\$/ton, with purity of 70–95%) [35].

Experimental

Fabrication of NG/PDMS rubber composites

NG/PDMS rubber composite samples were prepared from natural graphite of 100 mesh (Vonder) and Sylgard 184 silicone elastomer (Dow Corning). The purity of the natural graphite was evaluated by X-ray diffraction (Fig. S1 in Electronic Supplementary Material, ESM). The pre-polymer base and the curing agent were mixed together at the recommended mass proportion of 10:1, respectively. The fillers of natural graphite were added and homogenized into the uncured PDMS, varying the concentration from 0 (no filler, i.e. pure PDMS) to 40 wt%. The mixed uncured PDMS with natural graphite was poured into aluminum molds and degassed in low vacuum, for 45 min. The samples were cured using a digital oven at 368 K, for 50 min, then naturally cooled out of the oven, and finally removed from the molds using isopropyl alcohol. (See Fig. S2 in ESM for an example of 40 wt% NG/PDMS rubber composite and pure PDMS rubber).

Shore hardness test

Shore hardness tests of the samples were performed using a shore durometer from Instrutherm, model DP-100, which measures Type-A hardness, following ASTM D2240-15. Each testing specimen was prepared with a diameter of 40 mm and thickness of 10 mm and was measured ten times (five times at the top and five times at the bottom).

Density test

The density (ρ) of the samples was estimated by a 10-mL pycnometer, using ultrapure distilled water, whose density at ambient pressure and temperature (~ 295 K) is 997.8 kg m^{-3}. Each testing specimen was prepared with a diameter of 8 mm and length of 20 mm and was measured ten times.

Specific heat from differential scanning calorimetry

Specific heat (c_p) as a function of temperature was determined for PDMS, NG/PDMS composites, and natural graphite (as powder and pressed powder) using a commercial differential scanning calorimetry (NETZSCH, model DSC 214 Polyma). The runs were performed in heating and cooling processes, with minimum (T_{min}) and maximum (T_{max}) temperatures of 113 and 373 K, respectively, starting from room temperature (T_0). The temperature rate was 10 K min^{-1}, with 40 mL min^{-1} of N$_2$ flow. The runs followed the sequence: $T_0 \rightarrow T_{max} \rightarrow T_{min} \rightarrow T_{max} \rightarrow T_0$. The samples had ~ 10 mg and were placed in an aluminum pan with a holed lid. Sensitivity calibration was performed with sapphire of 12.5 mg, according to the manufacturer's manual; the data from the second heating ($T_{min} \rightarrow T_{max}$) were used in the calculations.

Thermal diffusivity test and thermal conductivity

Thermal diffusivity (α) tests were performed using a homemade diffusimetry, which consists of two thermal reservoirs (293 and 303 K), where the specimen is dipped from one to another. The testing specimens were prepared as a hollow cylinder with a length of 90 mm, an outer diameter of 15 mm, and an inner diameter of 1 mm. A K-type thermocouple of 1-mm

diameter was inserted through the inner hole and positioned at 45 mm in length. Temperature versus time data was recorded by a temperature controller (Lake Shore Cryotronics, Model 335) and then analyzed as an infinite cylinder subject to transient conduction [36]. Each sample was transferred five times from the hot reservoir to the cold reservoir, and another five times from the cold reservoir to the hot reservoir. Thermal conductivity (κ) of the samples was calculated by $\kappa = \alpha \rho c_p$.

Direct measurement of temperature change

Direct measurement of temperature change (ΔT) was performed in a similar experimental setup detailed elsewhere [37]. An upgrade was accomplished by automating via LabView different processes in a universal testing machine, which made it versatile to evaluate mechanical, barocaloric, and other thermal properties (See Fig. S3 in ESM for details). In compression or decompression process for ΔT data, pressure varies quickly enough (~ 4 s) to preclude significant heat exchange between the sample and its surroundings, which can be approximated as a quasi-adiabatic process. ΔT was systematically measured as a function of temperature (range of 223–333 K) and pressure change (range of 50–390 MPa), in samples of 8-mm diameter and 20-mm length.

Mechanical pressure test

Pressure (p) versus volumetric strain ($\varepsilon_v = \frac{\Delta V}{V_0}$, where V is volume) was measured in a quasi-isothermal process (maximum temperature variation was less than 1 K), on the universal testing machine operating at low speed of 1 mm min^{-1}. Data were recorded at an initial temperature of 303 K, in a compression-decompression cycle, with minimum pressure of ~ 2 MPa and maximum pressure of 390 MPa. In addition, it was possible to estimate the bulk modulus ($B = \left(\frac{\partial p}{\partial \varepsilon_v}\right)_T$) by numerical differentiation.

Thermal expansion coefficient test

The thermal expansion coefficient test was also performed on the mechanical testing machine, modified to be a dilatometer in isobaric conditions. The temperature was varied around room temperature (T_0), between the maximum temperature (T_{max}) of 333 K and the minimum temperature (T_{min}) of 213 K, on heating and cooling processes. The runs were performed with temperature rate of 4 K min^{-1} (following ISO 11359), according to $T_0 \rightarrow T_{max} \rightarrow T_{min} \rightarrow T_{max}$. The data analyzed to estimate the coefficient of thermal expansion ($CTE = \left(\frac{\partial \varepsilon_v}{\partial T}\right)_p$) were from the last two processes.

Results and discussion

During the demolding of PDMS and the NG/PDMS composites, it was interesting to realize some changes in mechanical properties among the samples. An increase in hardness was evaluated on Shore A scale, as shown in Table 1. Although the hardness does not follow a linear trend (Fig. S4 in ESM), there was a tendency to increase it as the concentration of natural graphite increases. For the maximum concentration of 40 wt% of natural graphite, the increase in Shore A hardness was $\sim 38\%$ compared to PDMS.

Other mechanical properties were also evaluated in pressure versus volumetric strain curves (Fig. 1a). Firstly, the viscoelastic behavior was evidenced by

Table 1 Properties of PDMS and NG/PDMS composites

Sample	Hardness (shore A)	ρ (kg m^{-3})	c_p (J kg^{-1} K^{-1})	$CTE \times 10^4$ (K^{-1})	$\alpha \times 10^7$ (m^2 s^{-1})	κ (W m^{-1} K^{-1})
PDMS	50(1)	1022(4)	1363(7)	8.3(1)	1.18(2)	0.164(3)
10wt% NG/PDMS	58(2)	1073(2)	1312(9)	7.6(2)	1.85(5)	0.260(7)
20wt% NG/PDMS	62(2)	1139(2)	1266(14)	7.3(2)	2.57(6)	0.37(1)
30wt% NG/PDMS	67(2)	1158(2)	1221(28)	6.8(3)	4.9(2)	0.69(3)
40wt% NG/PDMS	69(2)	1212(5)	1091(29)	6.1(2)	7.3(5)	0.97(7)

ρ is density at ~ 295 K and ambient pressure; c_p is specific heat at 220–330 K and ambient pressure; CTE is coefficient of thermal expansion at 223–333 K and ambient pressure; α is thermal diffusivity at 298 K and ambient pressure; κ is thermal conductivity calculated by $\kappa = \alpha \rho c_p$. The uncertainty for the last digits is shown in parentheses
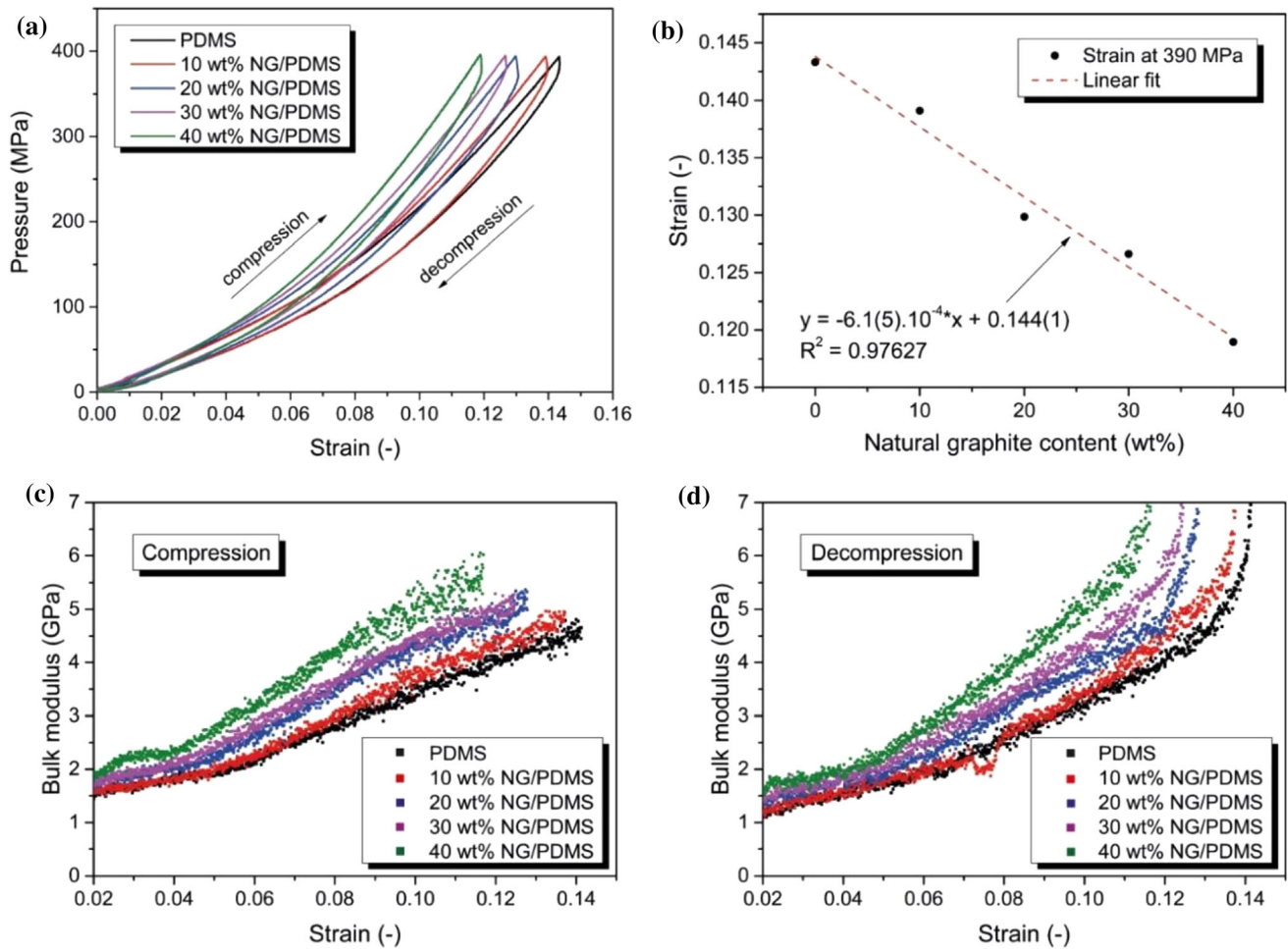
Figure 1 Mechanical properties of PDMS and NG/PDMS composites. **a** Pressure versus strain in a compression–decompression cycle. **b** Strain at 390 MPa versus natural graphite content; the black circles are experimental data and the red dashed line is the linear fit of the experimental data. **c** Bulk modulus versus strain during compression process. **d** Bulk modulus versus strain during decompression process.

the hysteresis loop defined by the compression and decompression curve. This behavior was expected because viscoelastic polymers dissipate heat during a closed compression–decompression cycle; such hysteresis loops were similar for all samples, reaching 3.2(3) GJ m^{-3} of dissipated heat. The samples were also similar for pressures below 50 MPa, but they behaved differently for pressures above 50 MPa. As the concentration of natural graphite increased, the samples tended to deform less at high pressures. For the maximum load of 390 MPa, for example, the composite with 40 wt% of natural graphite deformed ∼ 17% less than PDMS (Fig. 1b). In other words, composites with higher concentrations of natural graphite showed higher bulk moduli; this can be observed in Fig. 1c and d. Although the bulk
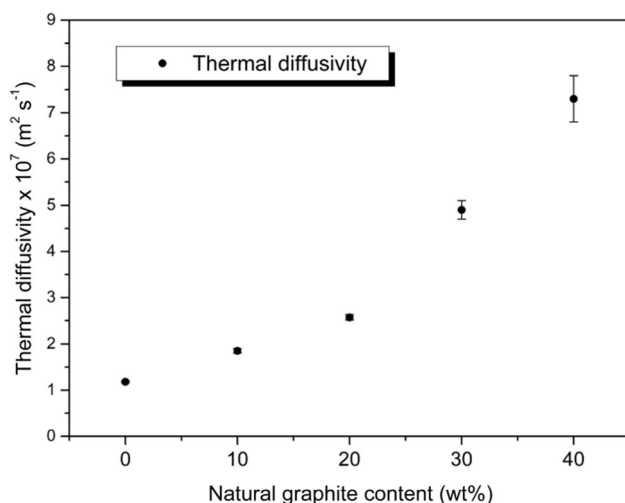
modulus curves are noisy, it was possible to observe a tendency to increase the bulk modulus when the composites were more deformed, a behavior that is typical of elastomers. For the bulk moduli values larger than 6 GPa that occur during the decompression process (Fig. 1d), they are not intrinsic to that specific strain range and are due to the slow response in deformation when the pressure starts to be relieved, as seen in pressure-strain curves for decompression (Fig. 1a). In other words, these values of bulk moduli larger than 6 GPa are artifacts of the numerical derivative at the limits of the hysteresis loop attributed to the viscoelastic behavior of PDMS.

The density obtained by pycnometry for PDMS was 1022(4) kg m^{-3}, against the maximum of 1212(5) kg m^{-3} for the 40 wt% NG/PDMS, that is, an increase

of ∼ 19% (Table 1). In general, the density values followed a linear trend (Fig. S5 in ESM) and were among the expected values, because the density reported in the catalog of Sylgard 184 is 1030 kg m^{-3}, while Vonder's natural graphite can vary between 2100 and 2300 kg m^{-3}.

With the calorimetric measurements, it was possible to estimate the glass transition temperature (T_g) of PDMS and NG/PDMS composites and also their specific heats; Fig. S6 (ESM) illustrates these results for a heating process. It was observed that all samples presented T_g around 151 K, similar to the T_g around 150 K reported in the literature for different PDMS samples [38, 39]. The difference between the composites was essentially in specific heat, due to the low specific heat of the natural graphite. The mean values of specific heat in the range of 220–330 K, which were used to estimate the isothermal entropy change, are displayed in Table 1.

Another property investigated was the coefficient of thermal expansion (*CTE*), displayed in Table 1 and Fig. S7 (ESM). The addition of natural graphite linearly reduced the ability of the samples to deform with temperature. For PDMS, a *CTE* of 8.3(1) × 10^{-4} K^{-1} was obtained, against 6.1(2) × 10^{-4} K^{-1} for 40 wt% NG/PDMS, which is equivalent to a reduction of ∼ 27%. Despite this, the order of magnitude was 10^{-3}, which is considerably high for solid materials; high values of *CTE* are important because elastomers have giant barocaloric effects due to these characteristics.

The thermal diffusivity increased ∼ 500% from 1.18(2) × 10^{-7} m^2 s^{-1} for PDMS to 7.3(5) × 10^{-7} m^2 s^{-1} for 40 wt% NG/PDMS (Table 1). The increase in thermal diffusivity in relation to the increase in graphite concentration does not follow a linear trend (Fig. 2); this can be explained by the greater thermal contact between particles of natural graphite inside the matrix of composites with higher content of natural graphite. The thermal conductivity of PDMS is merely 0.164(3) W m^{-1} K^{-1}, while thermal conductivity increases to 0.260(7), 0.37(1), 0.69(3), and 0.97(7) W m^{-1} K^{-1}, for NG/PDMS composites with 10, 20, 30, and 40 wt% NG, respectively (Table 1).

Figure 3 displays the temperature change (ΔT) obtained in compression and decompression processes for PDMS and NG/PDMS composites. The results for PDMS are similar to those reported in the literature [23]; for example, a maximum value of $|\Delta T|$ = 28.5 K at 283 K for $|\Delta p|$ = 390 MPa was reported by Carvalho et al. [23], while in this work it was observed $|\Delta T|$ = 27.7 K under the same conditions. This difference between the ΔT values was expected because the process reported by Carvalho et al.[23] was performed on a manual hydraulic press, which can perform a process closer to the adiabatic condition (∼ 0.2 s for any decompression pressure change) than the automated process on the universal testing machine (∼ 4 s for any compression and decompression pressure change).

The change in slope observed in $|\Delta T|$ vs. T curves (mainly for higher pressures on PDMS and 10%wt NG/PDMS) is related to the glass transition, which shifts its temperature value with pressure. In such state, the mobility of the polymeric chains is drastically reduced when compared to the rubbery state. Since the $|\Delta T|$ in elastomers are strongly related to conformations and mobility of chains [26], it is expected that values of $|\Delta T|$ are reduced below T_g. Also, this behavior was previously observed in other elastomers, such as vulcanized natural rubber [22] and nitrile butadiene rubber[24].

The glass transition also influences $|\Delta T|$ of NG/PDMS composites, but such influence was less and less significant within the temperature range analyzed, as the concentration of natural graphite increased. Probably, the addition of natural graphite to the PDMS matrix resulted in a different pressure shift of T_g (i.e., dT_g/dp) for each composite. For a maximum of 40 wt% of natural graphite, the curves

Figure 2 Thermal diffusivity as a function of natural graphite content for PDMS and NG/PDMS composites.

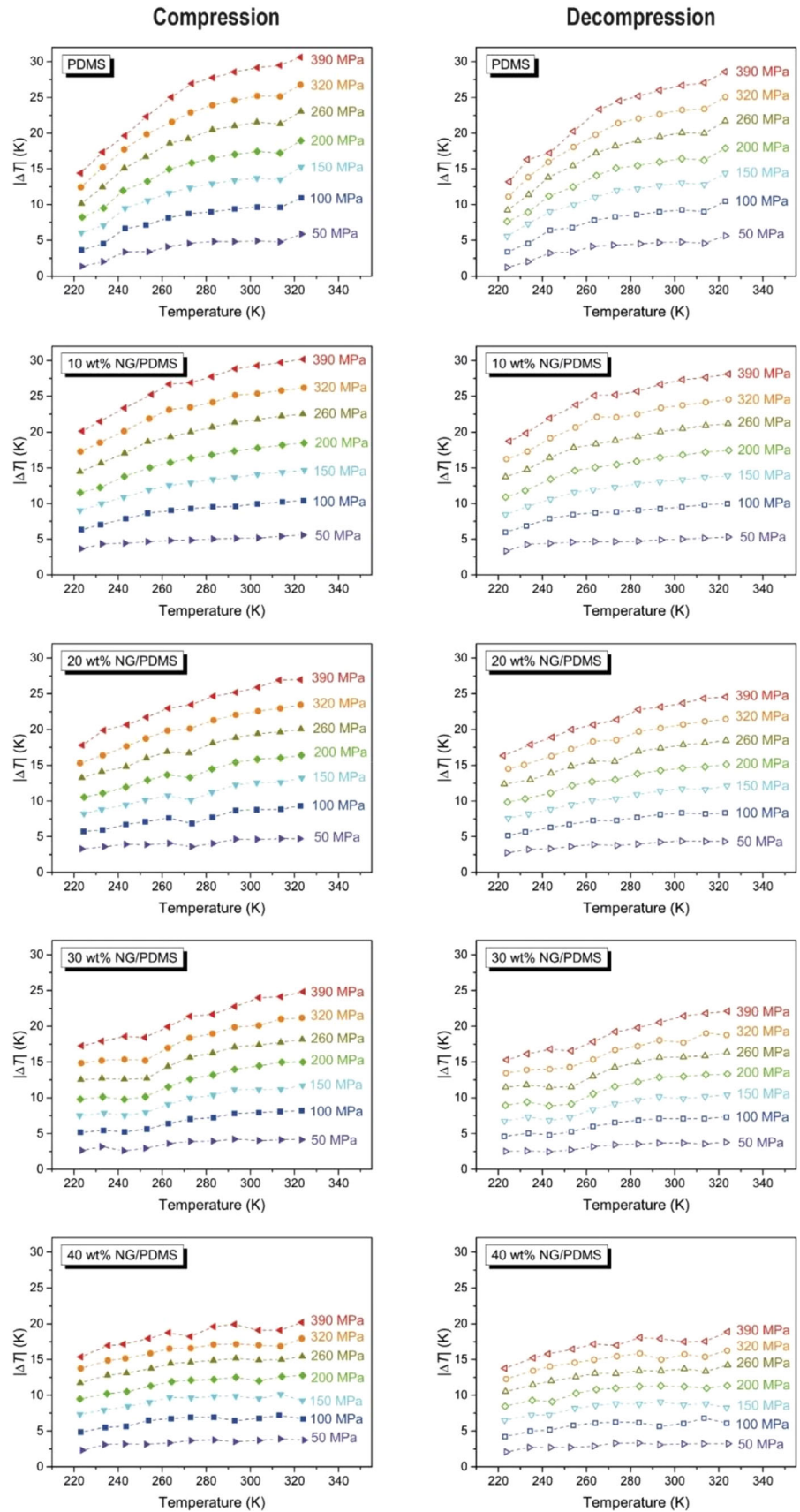**Figure 3** Temperature change (ΔT) versus temperature for PDMS and NG/PDMS composites, in compression process (closed symbols on the left) and decompression process (open symbols on the right), under pressure change (Δp) of 50(2), 100(3), 150(5), 200(6), 260(8), 320(10), and 390(12) MPa. Pressure errors were estimated at ± 3%. The dotted lines connecting the symbols are guides for the eyes.

Figure 4 Entropy change
(ΔS) versus temperature of
PDMS and NG/PDMS
composites, in compression
process (closed symbols on the
left) and decompression
process (open symbols on the
right), under pressure change
(Δp) of 50(2), 100(3), 150(5),
200(6), 260(8), 320(10), and
390(12) MPa. The ΔS was
calculated through the
equation $|\Delta S| = |\Delta T|c_p/T$,
using ΔT data from Fig. 3 and
c_p data from Fig. S6 and
Table 1. Pressure errors were
estimated at $\pm$ 3%. The dotted
lines connecting the symbols
are guides for the eyes.
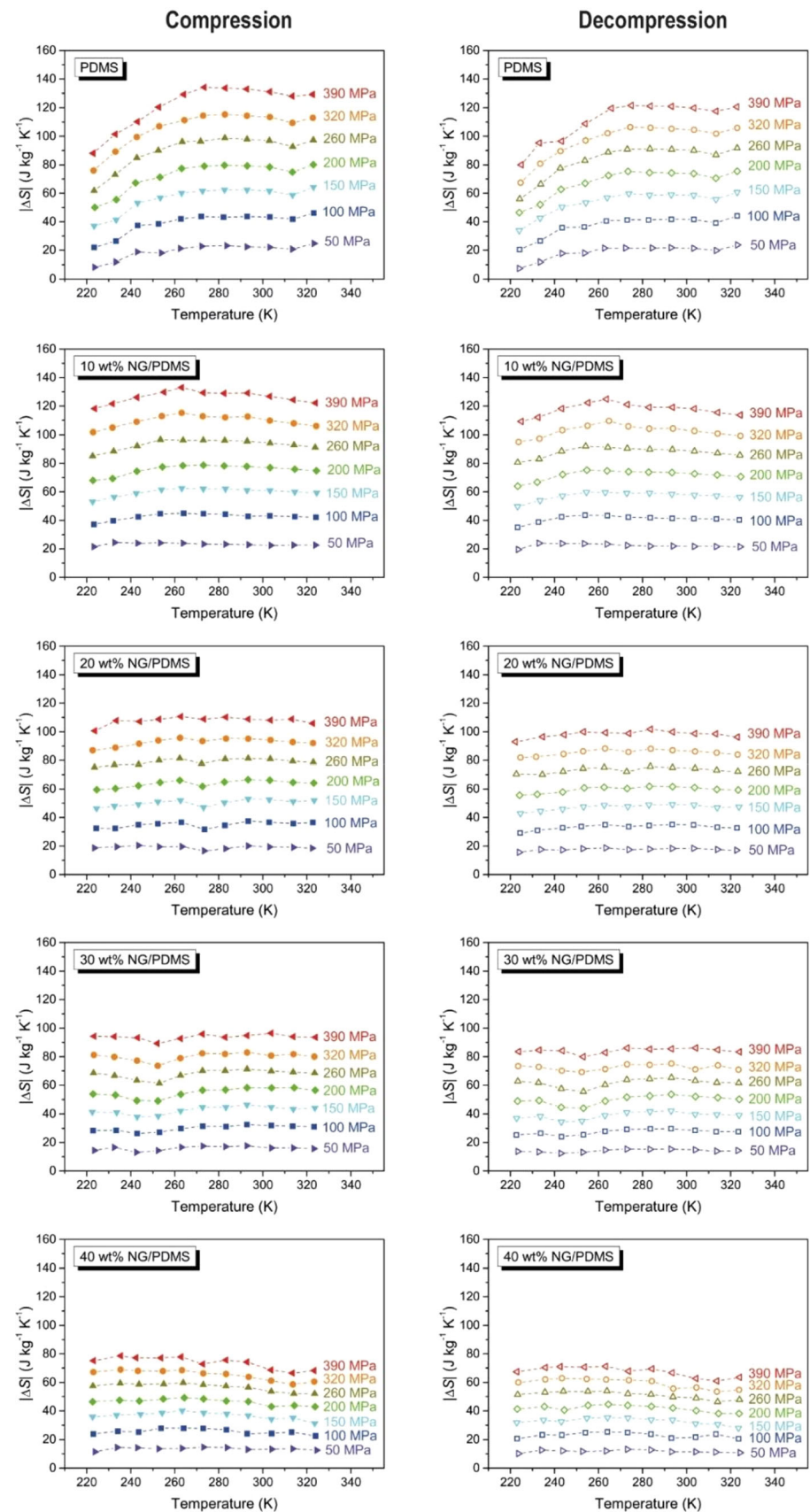
Table 2 Barocaloric properties of some promising materials for solid-state cooling devices

Barocaloric material	T (K)	Δp (GPa)	ΔT (K)	$\lvert\Delta T/\Delta p\rvert$ (K GPa^{-1})	$\lvert\Delta S\rvert$ (J kg^{-1} K^{-1})	$\lvert\Delta S/\Delta p\rvert$ (J kg^{-1} K^{-1} GPa^{-1})	Reference
PDMS	323	−0.39	− 28.6	73.3	120.6	309.3	This work
10 wt% NG/PDMS	323	−0.39	−28.0	71.8	113.7	291.5	This work
20 wt% NG/PDMS	323	−0.39	−24.6	63.1	96.2	246.7	This work
30 wt% NG/PDMS	323	−0.39	−22.1	56.7	83.3	213.6	This work
40 wt% NG/PDMS	323	−0.39	−18.7	47.9	63.5	162.8	This work
PDMS	273	−0.39	−24.4	62.6	121.6	311.7	This work
10 wt% NG/PDMS	273	−0.39	−25.2	64.6	121.1	310.5	This work
20 wt% NG/PDMS	273	−0.39	−21.2	54.4	98.8	253.2	This work
30 wt% NG/PDMS	273	−0.39	−19.2	49.2	86.0	220.5	This work
40 wt% NG/PDMS	273	−0.39	−16.9	43.3	67.8	173.7	This work
PDMS	223	−0.39	−13.2	33.8	79.9	204.9	This work
10 wt% NG/PDMS	223	−0.39	−18.4	47.2	109.2	279.9	This work
20 wt% NG/PDMS	223	−0.39	−16.4	42.1	92.9	238.3	This work
30 wt% NG/PDMS	223	−0.39	−15.2	39.0	83.5	214.1	This work
40 wt% NG/PDMS	223	−0.39	−13.8	35.4	67.4	172.7	This work
PDMS	304	−0.39	−28.2	72.3	146.0	374.4	[23]
PDMS	243	−0.39	−24.0	61.5	144.1	369.5	[23]
VNR	315	−0.39	−24.9	63.8	–	–	[22]
VNR	272	−0.39	−21.5	55.1	–	–	[22]
VNR	226	−0.39	−10.1	25.9	–	–	[22]
NBR	303	−0.173	−8.6	49.7	36.4	210.4	[24]
NBR	303	−0.39	−15.9	40.7	58.8	150.7	[24]
ASR	298	−0.39	−41.1	105.4	198.7	509.4	[27]
ASR	273	−0.39	−35.7	91.5	181.5	465.5	[27]
ASR	226	−0.39	−18.1	46.4	115.1	295.4	[27]
MnCoGe$_{0.99}$In$_{0.01}$	299	0.3	−9.4	31.3	–	–	[6]
MnCoGe$_{0.99}$In$_{0.01}$	299	0.3	−18.5^{i}	61.6^{i}	∼ 52	∼ 173	[6]
MnNiSi-FeCoGe	338	−0.2	3.1	15.5	–	–	[7]
MnNiSi-FeCoGe	338	0.25	−4.3	17.2	–	–	[7]
MnNiSi-FeCoGe	338	0.27	−16^{i}	59.3^{i}	∼ 70	∼ 259	[7]
Mn$_3$GaN	288	−0.093	1.32	14.2	–	–	[11]
Mn$_3$GaN	285	−0.093	4.8^{i}	51.6^{i}	∼ 21.5	∼ 231.2	[11]
(NH$_4$)$_2$SO$_4$	219	0.1	−8^{i}	80^{i}	∼ 60	∼ 600	[15]
Gd$_5$Si$_2$Ge$_2$	270	0.2	1.1	5.5	∼ 10.7	∼ 53.5	[8]
LaFe$_{11.33}$Co$_{0.47}$Si$_{1.2}$	237	−0.2	2.2	11	∼ 8.3	∼ 41.5	[9]
LaFe$_{11.33}$Co$_{0.47}$Si$_{1.2}$	239	−0.1	1.5	15	∼ 5	∼ 50	[9]
Fe$_{49}$Rh$_{51}$	313	0.25	10.4^{i}	41.6^{i}	∼ 10.8	∼ 43.2	[10]
(TPrA)[Mn(dca)$_3$]	330	0.00689	5.0^{i}	725.7^{i}	37	5370	[18]
(NH$_4$)$_3$MoO$_3$F$_3$	320	0.5	14.7^{i}	29.4^{i}	14.0	28.0	[3]
Rb$_2$KFeF$_6$	246	0.5	17.4^{i}	34.8^{i}	15.5	31.0	[3]
Rb$_2$KTiOF$_5$	237	0.5	15.8^{i}	31.6^{i}	16.7	33.4	[3]
(NH4)$_3$MoO$_2$F$_4$	270	0.5	∼ 12^{i}	∼ 24^{i}	∼ 13	∼ 26	[4]
(NH4)$_3$WO$_2$F$_4$	201	0.5	∼ 10^{i}	∼ 20^{i}	∼ 13.3	∼ 26.6	[4]
AgI	390	−0.25	∼ 18^{i}	∼ 72^{i}	∼ 60	∼ 240	[16]
NPG	320	−0.25	−23.5^{i}	94.0^{i}	445	1780	[30]
NPG	320	−0.52	−43.8^{i}	84.2^{i}	500	961.5	[30]
NPA	∼ 240	−0.26	−16^{i}	61.5^{i}	290	1115	[31]
NPA	∼ 240	−0.58	−42^{i}	72.4^{i}	470	810	[31]

T is initial temperature; Δp is pressure change (positive for compression and negative for decompression); ΔT is temperature change at T and Δp. $\lvert\Delta T/\Delta p\rvert$ is normalized temperature change. ^{i} indirect methods

Table 3 Coefficient of performance of PDMS and NG/PDMS composites

Barocaloric material	COP for different pressures changes						
	50 MPa	100 MPa	150 MPa	200 MPa	260 MPa	320 MPa	390 MPa
PDMS	8.0	3.8	2.6	2.0	1.5	1.2	1.0
10 wt% NG/PDMS	8.3	4.0	2.7	2.0	1.6	1.3	1.1
20 wt% NG/PDMS	7.0	3.6	2.4	1.9	1.4	1.2	1.0
30 wt% NG/PDMS	6.9	3.4	2.2	1.7	1.3	1.1	0.9
40 wt% NG/PDMS	5.4	2.9	2.0	1.5	1.2	1.0	0.8

The *COP* was calculated using ΔS data from decompression process at 273 K (Fig. 4), density from Table 1 and pressure vs. strain data from Fig. 1a

for the same $|\Delta p|$ practically do not vary $|\Delta T|$ over a wide temperature range, meaning that dT_g/dp is lower when compared to PDMS.

The entropy change ($|\Delta S|$) showed in Fig. 4 was calculated through Maxwell's relation considering a c_p independent of pressure, following the well-known equation $|\Delta S| = |\Delta T| c_p/T$; this consideration is valid only far from transitions [40], which is the case of PDMS and NG/PDMS composites within the measured temperature range of 223–333 K.

The reduction of $|\Delta T|$ and $|\Delta S|$ values as the amount of NG increases is a trade-off for the gain in thermal performance (e.g., thermal diffusivity and conductivity). As well as the amount of the dispersed phase influences some properties that are intrinsically related to the barocaloric effect (e.g., bulk modulus and thermal expansion). Furthermore, NG may have an impact on reducing chain mobility of PDMS, and its contribution for $|\Delta T|$ and $|\Delta S|$ is expected to be low.

It is also important to mention that $|\Delta T|$ and $|\Delta S|$ values of NG/PDMS composite are in the class of giant barocaloric effects with large reversible values and in the absence of phase transitions, even for the

maximum concentration of 40 wt% of natural graphite. When comparing different values of ΔT and ΔS from NG/PDMS composites with ΔT and ΔS from other materials reported in the literature (Table 2), it is possible to conclude that NG/PDMS composite are great candidates for solid-state refrigeration. In general, ΔT values measured directly are higher or equivalent for different materials reported in the literature. The exceptions appear in two situations: (1) with ASR (acetic silicone rubber), which has a supergiant (or colossal) barocaloric effect due to combined effects of the first-order crystalline-amorphous transition and the polymer chain rearrangements unrelated to the crystallization process[27]; or (2) when there is a comparison with some materials evaluated by indirect methods. It is important to mention that indirect methods for ΔT tend to overestimate the measured values directly because the equations used always assume equilibrium conditions, which does not happen in practice (especially when there is a phase transition).

The energy efficiency of a barocaloric material was assessed by the Coefficient of Performance (COP) and the Normalized Refrigerant Capacity (NRC). The *COP* was evaluated as COP = $|Q/W|$, where $Q = T\Delta S$

Table 4 Normalized Refrigerant Capacity (*NRC*) of different barocaloric elastomer-based materials, at ΔT_{H-C} (temperature difference between hot and cold reservoirs) of 25 K

Barocaloric material	T_H (K)	Δp (MPa)	NRC (kJ kg^{-1} GPa^{-1})	Reference
PDMS	300	− 200	9.3[r]	This work
10 wt% NG/PDMS	300	− 200	9.2[r]	This work
20 wt% NG/PDMS	300	− 200	7.7[r]	This work
30 wt% NG/PDMS	300	− 200	6.6[r]	This work
40 wt% NG/PDMS	300	− 200	5.3[r]	This work
ASR	300	173	15.1[r]	[27]
VNR	315	173	8.3	[22]
NBR	315	173	5.2[r]	[24]

T_H is the temperature of the hot reservoir; Δp is the pressure change (positive for compression and negative for decompression). [r]obtained from reversible ΔS

is the useful heat removed by the sample and $W = \rho^{-1} \int_{\varepsilon_{v1}}^{\varepsilon_{v2}} p d\varepsilon$ is the work required for this. In Table 3, COP values of the composites at 273 K are assigned, for several pressure changes, considering the decompression ΔS data from Fig. 4, density from Table 1, and pressure vs. strain data from Fig. 1a. Since the theoretical performance limit for a Carnot refrigeration cycle ($\text{COP}_{\text{Carnot}} = \frac{T_C}{T_H - T_C}$) operating with a hot reservoir of $T_H = 300$ K and a cold reservoir of $T_C = 270$ K is 9, it is possible to observe again that NG/PDMS composites can be good candidates for solid-state refrigeration.

The NRC was calculated according to $NRC = \left| \Delta p^{-1} \int_{T_C}^{T_H} \Delta S dT \right|$ for different elastomer-based materials available in the literature, considering a temperature difference between T_H and T_C (i.e., $\Delta T_{H-C} = T_H - T_C$) of 25 K, as displayed in Table 4. In general, NG/PDMS composites presented NRC values better or equally comparable to insulating elastomers.

Finally, we propose a *Material Property Chart* (sometimes also called *Figure of Merit*) that presents a combination of properties that matter for solid-state cooling devices. This chart is built by plotting $|\Delta T|\gamma$
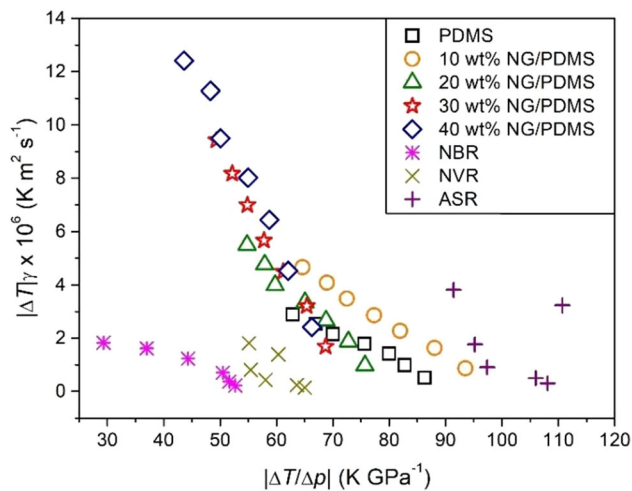
Figure 5 $|\Delta T|\gamma$ vs. $|\Delta T/\Delta p|$ at 273 K, in decompression process, for PDMS and NG/PDMS composites for $|\Delta p|$ of 50, 100, 150, 200, 260, 320 and 390 MPa; and NBR [24], NVR [22] and ASR [27] for $|\Delta p|$ of 26.0, 43.4, 86, 173, 273 and 390 MPa. $|\Delta p|$ values were not shown for the sake of clarity, but can be allocated for each material knowing that $|\Delta T|\gamma$ is directly proportional to $|\Delta p|$.

vs. $|\Delta T/\Delta p|$ because $|\Delta T|\gamma$ maximizes the rate of heat exchanged by the solid refrigerant in a refrigeration cycle and $|\Delta T/\Delta p|$ normalizes $|\Delta T|$ in order to avoid striking $|\Delta T|$ obtained from very high $|\Delta p|$. The resulting chart is helpful to organize promising barocaloric materials and also can suggest directions for further material development. As shown in Fig. 5, NG/PDMS composites again present better or similar performance among different barocaloric elastomers. It is important to highlight that the region near the upper-right corner is the ideal region of interest because it combines high values of $|\Delta T|\gamma$ with high values of $|\Delta T/\Delta p|$.

Conclusions

A systematic investigation of embedding natural graphite to PDMS rubber revealed that NG/PDMS rubber composites can combine giant barocaloric effects in a wide temperature range, and low and moderate pressure changes, in addition to improving the thermal conductivity and thermal diffusivity. NG/PDMS rubber composites presented giant barocaloric effects with a maximum reduction of $\sim 40\%$ in $|\Delta T|$ and $\sim 50\%$ in $|\Delta S|$ when compared to PDMS, but the thermal diffusivity increased $\sim 500\%$, from $1.18(2) \times 10^{-7}$ to $7.3(5) \times 10^{-7}$ m^2 s^{-1}, and the thermal conductivity, from 0.164(3) to 0.97(7) W m^{-1} K^{-1}. Our study evidences a promising potential of thermal-conductivity-based elastomer composites for solid-state cooling devices and should incite the development of other composites with different matrices (such as ASR or plastic crystals, which present supergiant or colossal barocaloric effect) embedded with different thermally conductive fillers (such as aluminum, copper, graphene, etc.), or even intermetallic compounds with different caloric effects, resulting in superior multi caloric materials.

Electronic supplementary material

See supplementary material for additional data on X-ray diffraction of natural graphite, sample's pictures, scheme of the barocaloric apparatus, shore hardness versus natural graphite content, density versus natural graphite content, specific heat curves for all samples and, coefficient of thermal expansion versus natural graphite content.

Acknowledgments

Author contributions

AMGC and ESNL conceived the study and led the project. WI, EOU, and AMGC planned the experiments. WI executed the experiments and analyzed the data. WI, EOU, AMGC, and ESNL wrote the paper.

Funding

Declarations

Conflict of interest The authors declare that they have no conflict of interest.

Supplementary Information: The online version contains supplementary material available at https://doi.org/10.1007/s10853-021-06649-9.

References

[1] Kitanovski A (2020) Energy applications of magnetocaloric materials. Adv Energy Mater 10:1903741. https://doi.org/10.1002/aenm.201903741

[2] Cazorla C (2019) Novel mechanocaloric materials for solid-state cooling applications. Appl Phys Rev 6:041316. https://doi.org/10.1063/1.5113620

[3] Flerov IN, Gorev MV, Tressaud A, Laptash NM (2011) Perovskite-like fluorides and oxyfluorides: phase transitions and caloric effects. Crystallogr Reports 56:9–17. https://doi.org/10.1134/S106377451101010X

[4] Gorev MV, Bogdanov EV, Flerov IN et al (2010) Investigation of thermal expansion, phase diagrams, and barocaloric effect in the $(NH_4)_2WO_2F_4$ and $(NH_4)_2MoO_2F_4$ oxyfluorides. Phys Solid State 52:167–175. https://doi.org/10.1134/S1063783410010294

[5] Flerov IN, Gorev MV, Bogdanov EV, Laptash NM (2016) Barocaloric effect in ferroelastic fluorides and oxyfluorides. Ferroelectrics 500:153–163. https://doi.org/10.1080/00150193.2016.1214525

[6] Wu RR, Bao LF, Hu FX et al (2015) Giant barocaloric effect in hexagonal Ni_2In-type Mn-Co-Ge-In compounds around room temperature. Sci Rep 5:18027. https://doi.org/10.1038/srep18027

[7] Samanta T, Lloveras P, Saleheen AU et al (2018) Barocaloric and magnetocaloric effects in $(MnNiSi)_{1-x}(FeCoGe)_x$. Appl Phys Lett 112:021907. https://doi.org/10.1063/1.5011743

[8] Yuce S, Barrio M, Emre B et al (2012) Barocaloric effect in the magnetocaloric prototype Gd5Si2Ge2. Appl Phys Lett 101:071906. https://doi.org/10.1063/1.4745920

[9] Mañosa L, González-Alonso D, Planes A et al (2011) Inverse barocaloric effect in the giant magnetocaloric La–Fe–Si–Co compound. Nat Commun 2:595. https://doi.org/10.1038/ncomms1606

[10] Stern-Taulats E, Gràcia-Condal A, Planes A et al (2015) Reversible adiabatic temperature changes at the magnetocaloric and barocaloric effects in Fe 49 Rh 51. Appl Phys Lett 107:152409–152412. https://doi.org/10.1063/1.4933409

[11] Matsunami D, Fujita A, Takenaka K, Kano M (2015) Giant barocaloric effect enhanced by the frustration of the anti-ferromagnetic phase in Mn 3 GaN. Nat Mater 14:73–78. https://doi.org/10.1038/nmat4117

[12] Stern-Taulats E, Lloveras P, Barrio M et al (2016) Inverse barocaloric effects in ferroelectric $BaTiO_3$ ceramics. APL Mater 4:091102. https://doi.org/10.1063/1.4961598

[13] Gorev MV, Mikhaleva EA, Flerov IN, Bogdanov EV (2019) Conventional and inverse barocaloric effects in ferroelectric NH_4HSO_4. J Alloys Compd 806:1047–1051. https://doi.org/10.1016/j.jallcom.2019.07.273

[14] Mikhaleva EA, Flerov IN, Gorev MV et al (2020) Features of the behavior of the barocaloric effect near ferroelectric phase transition close to the tricritical point. Curr Comput-Aided Drug Des, 10. https://doi.org/10.3390/cryst10010051

[15] Lloveras P, Stern-Taulats E, Barrio M et al (2015) Giant barocaloric effects at low pressure in ferrielectric ammonium sulphate. Nat Commun 6:8801. https://doi.org/10.1038/ncomms9801

[16] Aznar A, Lloveras P, Romanini M et al (2017) Giant barocaloric effects over a wide temperature range in superionic conductor AgI. Nat Commun 8:1851. https://doi.org/10.1038/s41467-017-01898-2

[17] Sagotra AK, Chu D, Cazorla C (2018) Room-temperature mechanocaloric effects in lithium-based superionic materials. Nat Commun 9:3337. https://doi.org/10.1038/s41467-018-05835-9

[18] Bermúdez-García JM, Sánchez-Andújar M, Castro-García S et al (2017) Giant barocaloric effect in the ferroic organic-inorganic hybrid [TPrA][Mn(dca)3] perovskite under easily accessible pressures. Nat Commun 8:15715–15722. https://doi.org/10.1038/ncomms15715

[19] Bermúdez-García JM, Sánchez-Andújar M, Señarís-Rodrı-guez MA (2017) A new playground for organic–inorganic hybrids: barocaloric materials for pressure-induced solid-state cooling. J Phys Chem Lett 8:4419–4423. https://doi.org/10.1021/acs.jpclett.7b01845

[20] Bermúdez-García JM, Yáñez-Vilar S, García-Fernández A et al (2018) Giant barocaloric tunability in [(CH$_3$CH$_2$CH$_2$)$_4$N]Cd[N(CN)$_2$]$_3$ hybrid perovskite. J Mater Chem C 6:9867–9874. https://doi.org/10.1039/c7tc03136j

[21] Reis MS (2020) Magnetocaloric and barocaloric effects of metal complexes for solid state cooling: review, trends and perspectives. Coord Chem Rev 417:213357. https://doi.org/10.1016/j.ccr.2020.213357

[22] Bom NM, Imamura W, Usuda EO et al (2018) Giant barocaloric effects in natural rubber: a relevant step toward solid-state cooling. ACS Macro Lett 7:31–36. https://doi.org/10.1021/acsmacrolett.7b00744

[23] Carvalho AMG, Imamura W, Usuda EO, Bom NM (2018) Giant room-temperature barocaloric effects in PDMS rubber at low pressures. Eur Polym J 99:212–221. https://doi.org/10.1016/j.eurpolymj.2017.12.007

[24] Usuda EO, Imamura W, Bom NM et al (2019) Giant reversible barocaloric effects in nitrile butadiene rubber around room temperature. ACS Appl Polym Mater 1:1991–1997. https://doi.org/10.1021/acsapm.9b00235

[25] Bom NM, Usuda ÉO, da Silva GM et al (2020) Waste tire rubber-based refrigerants for solid-state cooling devices. Chinese J Polym Sci 38:769–775. https://doi.org/10.1007/s10118-020-2385-y

[26] Miliante CM, Christmann AM, Usuda EO et al (2020) unveiling the origin of the giant barocaloric effect in natural rubber. Macromolecules 53:2606–2615. https://doi.org/10.1021/acs.macromol.0c00051

[27] Imamura W, Usuda ÉO, Paixão LS et al (2020) Supergiant barocaloric effects in acetoxy silicone rubber over a wide temperature range: great potential for solid-state cooling. Chinese J Polym Sci 38:999–1005. https://doi.org/10.1007/s10118-020-2423-9

[28] Li B, Kawakita Y, Ohira-Kawamura S et al (2019) Colossal barocaloric effects in plastic crystals. Nature 567:506–510. https://doi.org/10.1038/s41586-019-1042-5

[29] Li FB, Li M, Xu X et al (2020) Understanding colossal barocaloric effects in plastic crystals. Nat Commun 11:1–8. https://doi.org/10.1038/s41467-020-18043-1

[30] Lloveras P, Aznar A, Barrio M et al (2019) Colossal barocaloric effects near room temperature in plastic crystals of neopentylglycol. Nat Commun 10:1803. https://doi.org/10.1038/s41467-019-09730-9

[31] Aznar A, Lloveras P, Barrio M et al (2020) Reversible and irreversible colossal barocaloric effects in plastic crystals. J Mater Chem A 8:639–647. https://doi.org/10.1039/c9ta10947a

[32] Lloveras P, Tamarit J-L (2021) Advances and obstacles in pressure driven solid-state cooling: a review of barocaloric materials. MRS Energy Sustain, pp 1–18. https://doi.org/10.1557/s43581-020-00002-4

[33] Sadasivuni KK, Ponnamma D, Thomas S, Grohens Y (2014) Evolution from graphite to graphene elastomer composites. Prog Polym Sci 39:749–780. https://doi.org/10.1016/j.progpolymsci.2013.08.003

[34] Kwiecińska B, Petersen HI (2004) Graphite, semi-graphite, natural coke, and natural char classification–ICCP system. Int J Coal Geol 57:99–116. https://doi.org/10.1016/j.coal.2003.09.003

[35] Jara AD, Betemariam A, Woldetinsae G, Kim JY (2019) Purification, application and current market trend of natural graphite: a review. Int J Min Sci Technol 29:671–689. https://doi.org/10.1016/j.ijmst.2019.04.003

[36] Incropera FP (2006) Fundamentals of heat and mass transfer, 6th edn. Wiley, New York

[37] Bom NM, Usuda EO, Guimarães GM et al (2017) Note: Experimental setup for measuring the barocaloric effect in polymers: application to natural rubber. Rev Sci Instrum 88:046103–046105. https://doi.org/10.1063/1.4979464

[38] Mark JE (1999) Polymer data handbook. Oxford University Press

[39] Wolf MP, Salieb-Beugelaar GB, Hunziker P (2018) PDMS with designer functionalities—properties, modifications strategies, and applications. Prog Polym Sci 83:97–134. https://doi.org/10.1016/j.progpolymsci.2018.06.001

[40] Tishin AM, Spichkin YI (2003) The magnetocaloric effect and its applications. Institute of Physics Publishing